Radiology

A Comparison of Methods for High-Spatial-Resolution Diffusion-weighted Imaging in Breast MRI

Jessica A. McKay, PhD • An L. Church, MD • Nathan Rubin, MS • Tim H. Emory, MD • Noelle F. Hoven, MD • Jessica E. Kuehn-Hajder, MD • Michael T. Nelson, MD • Sudhir Ramanna, MS • Edward J. Auerbach, PhD • Steen Moeller, PhD • Patrick J. Bolan, PhD

From the Department of Biomedical Engineering (J.A.M., P.J.B.), Center for Magnetic Resonance Research (J.A.M., S.R., E.J.A., S.M., P.J.B.), Department of Radiology (A.L.C., T.H.E., N.F.H., J.E.K.H., M.T.N., S.R., E.J.A., S.M., P.J.B.), and Biostatistics Core, Masonic Cancer Center (N.R.), University of Minnesota, Center for Magnetic Resonance Research, 2021 6th St SE, Minneapolis, MN 55455. Received January 31, 2020; revision requested March 23; revision received May 15; accepted June 18. **Address correspondence to** J.A.M. (e-mail: *mckay203@umn.edu*).

Study supported by the National Center for Advancing Translational Sciences of the National Institutes of Health (UL1-TR002494) and the National Institutes of Health (NIH P41 EB027061, NIH S10OD017974-01, and NIH R21CA201834). The content is solely the responsibility of the authors and does not necessarily represent the official views of the National Institutes of Health.

Conflicts of interest are listed at the end of this article.

See also the editorial by Partridge in this issue.

Radiology 2020; 297:304–312 • https://doi.org/10.1148/radiol.2020200221 • Content code: BR

Background: Diffusion-weighted imaging (DWI) shows promise in detecting and monitoring breast cancer, but standard spin-echo (SE) echo-planar DWI methods often have poor image quality and low spatial resolution. Proposed alternatives include readout-segmented (RS) echo-planar imaging and axially reformatted (AR)–simultaneous multislice (SMS) imaging.

Purpose: To compare the resolution and image quality of standard SE echo-planar imaging DWI with two high-spatial-resolution alternatives, RS echo-planar and AR-SMS imaging, for breast imaging.

Materials and Methods: In a prospective study (2016–2018), three 5-minute DWI protocols were acquired at 3.0 T, including standard SE echo-planar imaging, RS echo-planar imaging with five segments, and AR-SMS imaging with four times slice acceleration. Participants were women undergoing breast MRI either as part of a treatment response clinical trial or undergoing breast MRI for screening or suspected cancer. A commercial breast phantom was imaged for resolution comparison. Three breast radiologists reviewed images in random order, including clinical images indicating the lesion, images with b value of 800 sec/mm^2, and apparent diffusion coefficient (ADC) maps from the three randomly labeled DWI methods. Readers measured the longest dimension and lesion-average ADC on three DWI methods, reported measurement confidence, and rated or ranked the quality of each image. The scores were fit to a linear mixed-effects model with intercepts for reader and subject.

Results: The smallest feature (1 mm) was only detectible in a phantom on images from AR-SMS DWI. Thirty lesions from 28 women (mean age, 50 years ± 13 [standard deviation]) were evaluated. On the five-point Likert scale for image quality, AR-SMS imaging scored 1.31 points higher than SE echo-planar imaging and 0.74 points higher than RS echo-planar imaging, whereas RS echo-planar imaging scored 0.57 points higher than SE echo-planar imaging (all $P < .001$).

Conclusion: The axially reformatted simultaneous multislice protocol was rated highest for image quality, followed by the readout-segmented echo-planar imaging protocol. Both were rated higher than the standard spin-echo echo-planar imaging.

Online supplemental material is available for this article.

Diffusion-weighted imaging (DWI) measures the apparent diffusion coefficient (ADC) of tissue, which is often lower because of cancer. There is growing interest in the use of DWI for breast cancer imaging for screening, disease characterization, and monitoring treatment response (1). DWI is typically acquired by using single-shot spin-echo (SE) echo-planar imaging, which faces several challenges that are often exacerbated in breast imaging because of the large field of view, adipose signal, and respiratory motion that alters the B_0 field. Standard breast DWI has low spatial resolution, large geometric distortions, chemical shift artifacts, and Nyquist ghost artifacts, which can limit its clinical value. Higher spatial resolution may also enable the use of DWI for additional analyses, including minimum ADC, DWI radiomics, histogram analysis, and rim sign (2,3).

Several strategies to improve the image quality of SE echo-planar imaging in breast DWI have been explored, including readout segmentation (RS) (4–7), reduced field of view (8,9), and multiband encoding in the phase encoding direction (10). A proposed strategy uses simultaneous multislice (SMS) imaging (11–13) to improve image quality in breast DWI (14–16). Because the SMS potential is greater in the right-to-left directions based on the coil geometry, this approach acquires sagittal images with aggressive SMS to cover a large volume with many thin slices. The images are axially reformatted (AR) for interpretation, according to standard clinical practice. Thus, the axial images are encoded by the readout and slice directions, which provides high in-plane resolution whereas the blurred and artifact-prone phase encoding direction is rotated through-plane.

In this study, we compared the image quality and resolution of standard SE echo-planar imaging breast DWI with two high-spatial-resolution imaging protocols on the basis of RS echo-planar imaging and AR-SMS imaging,

Abbreviations

ADC = apparent diffusion coefficient, AR = axially reformatted, DWI = diffusion-weighted imaging, I-SPY 2 = Investigation of Serial Studies to Predict Your Therapeutic Response with Imaging and Molecular analysis 2, RS = readout segmentation, SE = spin echo, SMS = simultaneous multislice

Summary

Axially reformatted simultaneous multislice imaging produced diffusion-weighted images and apparent diffusion coefficient maps with improved image quality, resolution, and coverage compared with a readout-segmented echo-planar imaging strategy and standard spin-echo echo-planar imaging.

Key Results

- For breast diffusion-weighted imaging, axially reformatted (AR)–simultaneous multislice (SMS) imaging provided the highest spatial resolution, covered the largest volume, and helped to detect the smallest feature (1 mm) compared with readout-segmented (RS) echo-planar imaging and standard spin-echo (SE) echo-planar imaging.
- By using the five-point Likert scale for image quality, AR-SMS imaging scored 1.31 points higher than SE echo-planar imaging and 0.74 points higher than RS echo-planar imaging whereas RS echo-planar imaging scored 0.57 points higher than SE echo-planar imaging (all $P < .001$).

with each optimized to provide full bilateral coverage in a clinically acceptable (<5 minute) imaging time. The three protocols were characterized with phantom resolution measurements, and in vivo performance was assessed by using a multireader study.

Materials and Methods

Study Participants

In this prospective institutional review board–approved and Health Insurance Portability and Accountability Act–compliant study, women undergoing clinical breast MRI at our imaging center were offered additional diffusion imaging to be acquired after their clinical examination between December 2016 and December 2018. Participants underwent breast MRI either as part of a treatment response clinical trial (Investigation of Serial Studies to Predict Your Therapeutic Response with Imaging and Molecular analysis 2 [I-SPY 2] trial) or clinical MRI for screening or for suspected cancer and provided written informed consent. Data from I-SPY 2 may be included in other studies (*clinicaltrials.gov* NCT01042379, NCT02058758), excluding RS echo-planar imaging and AR-SMS imaging.

Phantom Acquisition for Resolution Assessment

A commercial breast phantom (Model 131; CaliberMRI, Boulder, Colo) (17) with a resolution test grid was imaged with all DWI protocols. The phantom was rotated to assess the resolution in each plane. Feature detection was subjectively assessed (J.A.M., with 6 years of experience, and P.J.B., with 21 years of experience).

MRI Scan Acquisition

All images were acquired with a 3-T system (Siemens Prismafit; Siemens Healthcare, Erlangen, Germany) by using a 16-channel breast coil (Sentinelle; Philips Medical Systems, Hamburg, Germany). For every participant, standard MRI scans were acquired, including T2-weighted and a contrast agent–enhanced T1-weighted series with an intravenous injection of gadolinium-based contrast agent (gadobutrol, 0.1 mM/kg). RS echo-planar images and AR-SMS images were acquired after clinical imaging was completed. See Appendix E1 (online) for details.

Three different SE echo-planar imaging strategies were used to perform bilateral breast DWI. Whereas not fixed in resolution or volumetric coverage, each protocol was individually optimized for a 5-minute acquisition time. The first, Standard-A, represented the standard clinically available breast MRI by using single-shot SE echo-planar imaging compliant with the American College of Radiology Imaging Network, known as ACRIN, 6698 clinical trial (18) with nominal resolution of 1.7 mm × 1.7 mm × 4 mm. Because of time restrictions of clinical imaging, a shorter version with fewer b values, Standard-B, was used for participants undergoing clinical breast MRI (nontrial). The vendor's implementation was used for RS echo-planar imaging with protocol parameters on the basis of Wisner et al (5), chosen for its high and nearly isotropic resolution, with five readout segments and nominal resolution of 1.8 mm × 1.8 mm × 2.4 mm. AR-SMS imaging was implemented by modifying the custom SMS echo-planar imaging acquisition and reconstruction pipeline developed for the Human Connectome Project (19). The AR-SMS image acquisition used a four-time slice acceleration for 1.25-mm isotropic axial resolution and 2.5 mm through-plane (phase encoding) interpolated to 1.25 mm and included an additional reference examination with opposite phase encoding for geometric distortion correction (20). See Table 1 for protocol details.

Preparing Data Set for Reader Analysis

The MRI system vendor's image reconstructions were used for clinical acquisitions, standard SE echo-planar DWI, and RS echo-planar DWI. AR-SMS reconstruction was performed offline in Matlab R2017b (Mathworks, Natick, Mass) by using in-house reconstruction (Appendix E1 [online]). All images were transferred to a clinical picture archiving and communication system (iSite; Philips Healthcare, Andover, Mass) for analysis.

For each participant, a single study was chosen with preference for pretreatment examinations when available. By using T2-weighted and contrast-enhanced subtraction images, all contrast-enhanced, mass-like lesions within each DWI field of view were identified and their length was measured. The largest lesion from every woman was included, and secondary lesions from distant sections were included from two women.

Reader Analysis

Two lesions of different sizes were used to train the breast radiologists. The remaining lesions were independently presented to three radiologists (T.H.E., N.F.H., and J.E.K.H., with 19, 3, and 14 years of breast MRI experience, respectively) in random order in one or two (separated by < 7 days) sessions. The radiologists were blinded to the participant and the DWI

Table 1: Acquisition Parameters

	DWI				Clinical Examination		
	Standard SE Echo-planar Imaging					Contrast-enhanced T1-weighted Imaging	
Parameter	Standard-A	Standard-B	RS Echo-planar Imaging	AR-SMS	T2-weighted Imaging	I-SPY 2 (Standard-A)	Clinical (Standard-B)
Type of imaging	Single-shot SE echo-planar imaging	Single-shot SE echo-planar imaging	SE echo-planar imaging (5)*	Single shot SE echo-planar imaging	SE	3D gradient echo	3D gradient echo
TR (msec)	8000	8000	7800	6500	4500	4.72	4.72
TE (msec)	74.0	74.0	64.0	60.80	72.0	1.82	1.82
Phase encoding	R/L	R/L	AP	H/F	R/L	R/L	R/L
Readout encoding	AP	AP	R/L	AP	AP	AP	AP
Slice orientation	Axial	Axial	Axial	Sagittal	Axial	Axial	Axial
Echo spacing (msec)	0.74	0.74	0.32	0.93	NA	NA	NA
No. of echoes acquired	48	48	43	38	NA	NA	NA
No. of averages	…	…	…	…	1	1	1
b values (no. of averages)†							
0 sec/mm²	5 (1)	5 (1)	3 (1)	4 (1)	…	…	…
100 sec/mm²	3 (3)	3 (3)	…	…	…	…	…
600 sec/mm²	3 (3)	…	…	…	…	…	…
800 sec/mm²	3 (3)	3 (3)	2 (3)	8 (3)	…	…	…
Diffusion scheme	Bipolar	Bipolar	Bipolar	Monopolar	…	…	…
Nominal resolution (mm)‡	1.7 × 1.7	1.7 × 1.7	1.8 × 1.8	1.25 × 2.5	0.8 × 0.8	0.6 × 0.6	0.6 × 0.6
Coverage (mm)							
R/L	320	320	350	320	320	300–340	300–340
AP	320	320	156	240	320	300–340	300–340
H/F	144–176	144–176	134.4	240	198	208	208
No. of slices	36–44	44	56	256	60	160	160
Slice thickness (mm)	4	4	2.4	1.25	3.0	1.3	1.3
Slice gap (mm)	0	0	0	0	0.3	…	…
GRAPPA	3	3	2	2	2	3	3
SMS	…	…	…	4	…	…	…
Partial Fourier							
Phase	6/8	6/8	None	6/8	…	6/8	6/8
Slice	…	…	None	…	…	6/8	6/8
Acquisition time (min)	4:58	3:46	4:58	4:52	4:59	1:32	1:58
No. of acquisitions	…	…	…	…	…	7	4

Note.—Standard-A was used for participants in the Investigation of Serial Studies to Predict Your Therapeutic Response with Imaging and Molecular analysis 2 (I-SPY 2) clinical trial; Standard-B, with fewer *b* values, was used for clinical participants not enrolled in I-SPY 2 to reduce total imaging time. All participants were additionally imaged with readout-segmented echo-planar imaging and axially-reformatted simultaneous multislice imaging. A/P = anteroposterior, AR = axially reformatted, DWI = diffusion-weighted imaging, FOV = field of view, GRAPPA = generalized autocalibrating partially parallel acquisitions, H/F = head/foot, NA = not applicable, PE = phase encoding, R/L = right/left, RO = readout, RS = readout segmented, SE = spin echo, SMS = simultaneous multislice imaging, TE = echo time, TR = repetition time, 3D = three-dimensional.

* Data in parentheses are readout segments.

† Data in parentheses are number of directions.

‡ Data are readout × phase encoding.

method. For each lesion, the radiologists were provided with clinical images, images with *b* value of 800 sec/mm², and ADC maps from all three DWI methods, presented axially in random order. The lesion was indicated on the contrast-enhanced subtraction, as shown in Figure 1.

The readers measured the longest dimension on the contrast-enhanced subtraction images and images with *b* values of 800 sec/mm² and lesion-average ADC by using a freehand two-dimensional region of interest on a representative section. Readers reported their confidence of these measurements by using

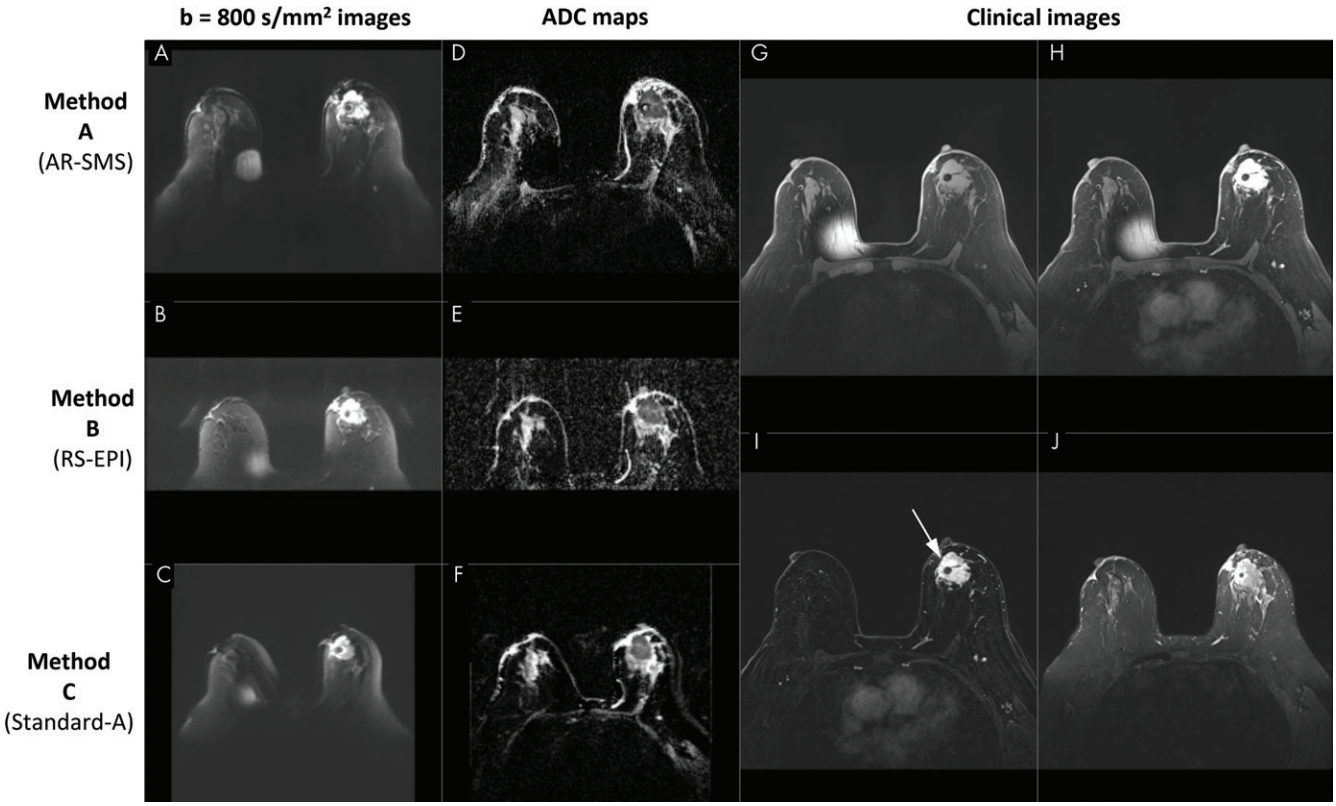

Figure 1: Screenshot of a picture archiving and communication system setup in a 70-year-old participant with large biopsy-proven cancer. Readers were provided with clinical images, including, *G*, a noncontrast-enhanced image, *H*, a single contrast-enhanced image, *I*, a contrast-enhanced subtraction T1-weighted image, and, *J*, a T2-weighted image, with the lesion indicated (arrow). Diffusion data included axial images with, *A–C*, *b* value of 800 sec/mm^2 and, *D–F*, apparent diffusion coefficient (ADC) maps for all three methods, randomly ordered as methods A, B, and C, which are labeled here for illustration purposes. The metal needle of the contrast injection port caused the artifact on the right breast. AR-SMS = axially reformatted–simultaneous multislice, RS-EPI = readout-segmented echo-planar imaging.

a five-point Likert scale from no confidence (1 point) to very high confidence (5 points). Readers reported their impression of overall image quality by using a scale of 1 (unusable) to 5 (excellent and equivalent to contrast-enhanced MRI) and ranked the methods (first through third).

Statistical Analysis

Scores were fit to a linear mixed-effects model including random intercepts for reader and participant to account for repeated measurements. The model was used to measure differences in the overall image quality, method rank, and confidence in length and ADC measurements on images from DWI. A second model was used, adding the effect of lesion size. Intraclass correlation (two-way random effects of type consistency and single) was used to determine the interreader consistency.

Whereas primary analysis was performed by combining Standard-A and Standard-B for larger data size, a subanalysis separately considered the image quality to confirm that the quality was comparable despite fewer *b* values used in Standard-B (Appendix E1 [online]).

We used statistical software (R version 3.6.0; R Core Team, Vienna, Austria) for this analysis. *P* values less than .05 after a Tukey adjustment for the three pairwise comparisons were considered to indicate statistically significant results (emmeans package in R).

Results

Participant Characteristics

Forty women (age rage, 27–78 years; mean age, 51 years ± 13 [standard deviation]) consented to and underwent additional DWI; of these, 30 women (age range, 27–78 years; mean age, 50 years ± 14) presented with contrast-enhanced lesions on contrast-enhanced subtraction images. Of 32 lesions identified for inclusion, two were used to train radiologists, leaving 30 lesions for analysis from 28 participants (Table 2).

Phantom

In the resolution phantom (Fig 2), the 1-mm feature was only considered detectable on the axial plane on AR-SMS and T2-weighted images. The 2-mm feature was detectable in the axial plane for all methods but was nearly undetectable in the sagittal plane of Standard-A.

Reader Analysis

Representative examples of large and small lesions are shown in Figures 3 and 4. All three readers rated AR-SMS images with the highest image quality and ranked AR-SMS images higher than both RS echo-planar images and standard SE echo-planar images, as shown in Figure 5.

Table 2: Inclusion and Demographics of Participants

Description	No. of Participants	Mean Age (y)	Mean BI-RADS Breast Density Score	Mean Lesion Length (mm)
Women offered research add-on for at least one examination	52	49 ± 14 (27–78)	2.8 ± 0.8 (1–4)	NA
Screening	18			
I-SPY 2	34			
Women who did not consent to research examinations at any time	4	51 ± 4 (47–55)	2.5 ± 0.6 (2–3)	NA
Screening	0			
I-SPY 2	4			
Women who consented to additional DWI scanning for at least one examination	48	49 ± 13 (27–78)	2.9 ± 0.8 (1–4)	NA
Screening	18			
I-SPY 2	30			
Women who consented for additional DWI but did not complete it at any examination	8	41 ± 3 (34–46)	3.1 ± 0.6 (2–4)	NA
Screening	2			
I-SPY 2	6			
Withdrew for discomfort	7			
Technical difficulties	1			
Women who completed additional DWI scanning for at least one examination	40	51 ± 13 (27–78)	2.8 ± 0.8 (1–4)	NA
Screening	16			
I-SPY 2	24			
Excluded for missing data	2	54 ± 9 (47–60)	2.0 ± 1.4 (1–3)	NA
Screening	1			
I-SPY 2	1			
Excluded for no qualifying lesion	8	55 ± 9 (44–70)	3.1 ± 0.8 (2–4)	N/A
Screening	7			
I-SPY 2	1			
Women with enhanced lesions on CE subtraction images included in study	30 (32)*	50 ± 14 (27–78)	2.8 ± 0.8 (1–4)	19.6 ± 13.3 (3.1–51.2)
Enrolled in I-SPY 2 with biopsy-proven cancer, before treatment†	12 (13)*	55 ± 14 (36–78)	2.8 ± 0.8 (2–4)	30.6 ± 9.6 (12.7–51.2)
Analysis	11			
Training	1			
Enrolled in I-SPY 2 with biopsy-proven cancer, after treatment†	10 (11)*	43 ± 16 (27–71)	2.8 ± 1.0 (1–4)	15.7 ± 13.7 (3.1–46.3)
Analysis	9			
Training	1			
Underwent MRI screening‡	8 (8)*	50 ± 6 (39–59)	2.8 ± 0.5 (2–3)	8.5 ± 5.3 (4.1–16.9)
Analysis	8			
Training	0			

Note.—Mean data are ± standard deviation. Unless otherwise indicated, data in parentheses are range. Age indicates age at enrollment in the study. Breast density was recorded according to the participant's medical records on the BI-RADS scale (1 = BI-RADS A [mostly fatty], 2 = BI-RADS B [scattered density], 3 = BI-RADS C [heterogeneous density], and 4 = BI-RADS D [extremely dense]). Any participant included twice was included for two unique lesions. Lesion length was measured on contrast-enhanced subtraction images on the basis of the average over three readers (lesions included in analysis) or measured by an MRI physicist (training cases). BI-RADS = Breast Imaging Reporting and Data System, CE = contrast enhanced, DWI = diffusion-weighted imaging, I-SPY 2 = Investigation of Serial Studies to Predict Your Therapeutic Response with Imaging and Molecular analysis 2.

* Data in parentheses are number of lesions.

† Underwent Standard-A DWI.

‡ Underwent Standard-B DWI.

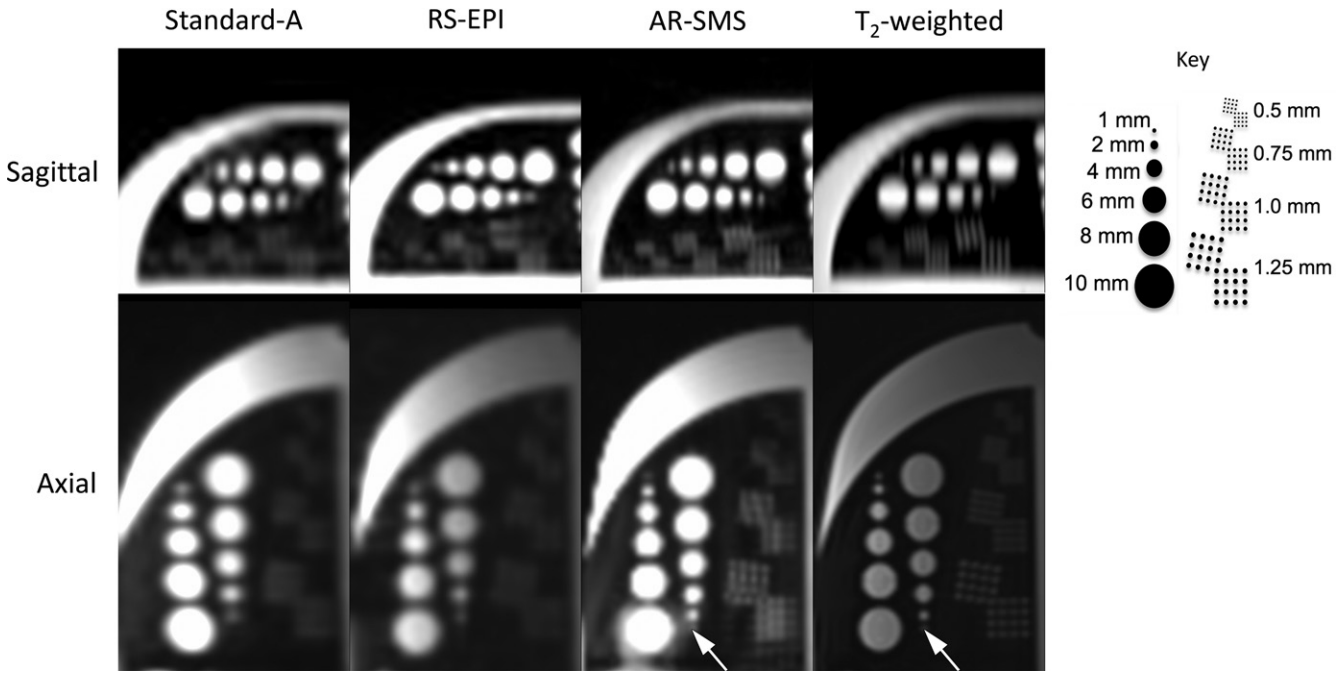

Figure 2: Resolution phantom comparing feature detection on $b = 0$ sec/mm^2 images. Key indicates feature sizes. The smallest feature (1 mm), indicated by an arrow, was only considered visible on the axially reformatted–simultaneous multislice (AR-SMS)and T2-weighted axial images. The 1 mm and 1.25 mm dots in the resolution grids are differentiable on axially reformatted simultaneous multislice and T2-weighted images. RS-EPI = readout-segmented echo-planar imaging.

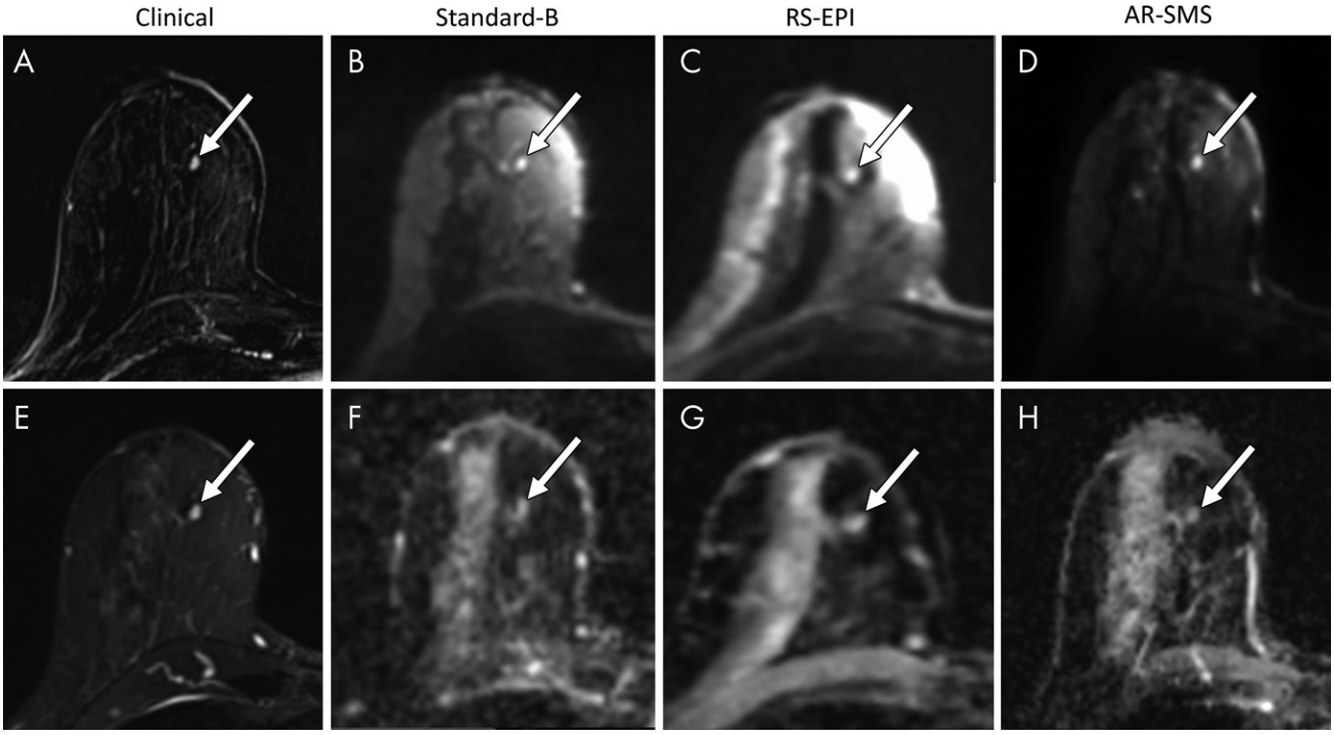

Figure 3: Small lesion example. Shown are, *A*, a contrast-enhanced subtraction image, *E*, a T2-weighted image, *B–D*, images with *b* value of 800 sec/mm^2, and, *F–H*, apparent diffusion coefficient (ADC) maps, focused on an example of a small contrast-enhanced lesion (arrow). Radiologists were asked to measure the longest dimension on images with *b* value of 800 sec/mm^2 (*B–D*) and a lesion-average ADC by drawing a freehand two-dimensional region of interest on each ADC map (*F–H*). The longest lesion diameter was 4.7 mm, measured on the contrast-enhanced subtraction image (*A*) and averaged across all readers. Average measurements on images with *b* value of 800 sec/mm^2 were as follows: *B*, standard, 5.8 mm; *C*, readout-segmented (RS) echo-planar imaging (EPI), 4.6 mm; and *D*, axially reformatted (AR)–simultaneous multislice (SMS) image, 5.5 mm. Average ADC measurements were as follows: *F*, standard, 1.45 × 10^{-3} mm^2/sec; *G*, RS echo-planar image, 1.59 ×10^{-3} mm^2/sec; and *H*, R-SMS image, 1.34 ×10^{-3} mm^2/sec. The average quality scores on a five-point LIkert scale were as follows: standard, 2.3; RS echo-planar imaging, 2.7; and AR-SMS imaging, 3.7.

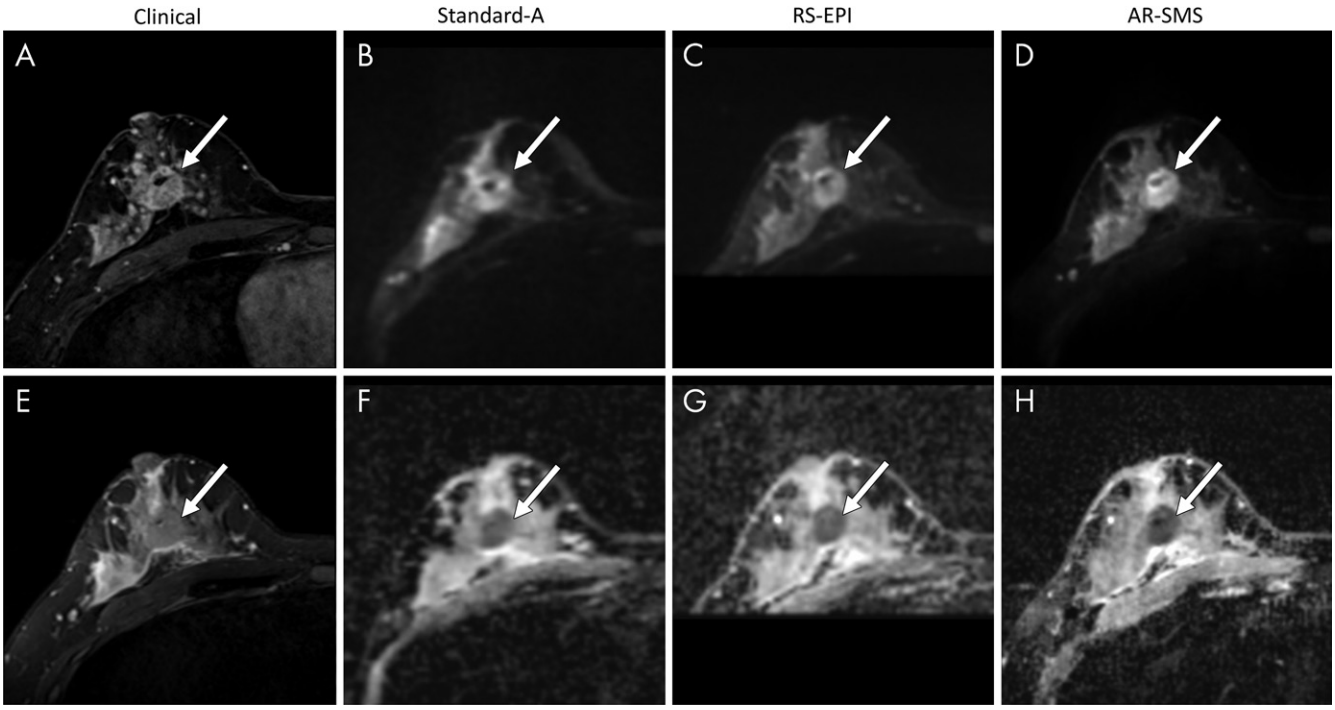

Figure 4: Large lesion example. Shown are, *A*, contrast-enhanced image, *E*, T2-weighted image, *B–D*, images with *b* value of 800 sec/mm^2, and, *F–H*, apparent diffusion coefficient (ADC) maps, which are focused on an example of a large contrast-enhanced lesion (arrow). Radiologists were asked to measure the longest dimension on (*B–D*) images with *b* value of 800 sec/mm^2 and (*F–H*) a lesion-average ADC by drawing a freehand two-dimensional region of interest on each ADC map. The longest lesion diameter was 28.8 mm, measured on the contrast-enhanced subtraction image and averaged across all readers. Average measurements on images with *b* value of 800 sec/mm^2 were as follows: *B*, standard, 26 mm; *C*, readout-segmented (RS) echo-planar imaging, 25.6 mm; and *D*, axially reformatted (AR)–simultaneous multislice (SMS) image, 26 mm. Average ADC measurements were as follows: *F*, standard, 0.88 $\times 10^{-3}$ mm^2/sec; *G*, RS echo-planar imaging, 0.93 $\times 10^{-3}$ mm^2/sec; and, *H*, AR-SMS imaging, 0.84 $\times 10^{-3}$ mm^2/sec. The average quality scores on a five-point Likert scale were as follows: standard, 2.3; RS echo-planar imaging, 3.0; and AR-SMS imaging, 4.0.

A

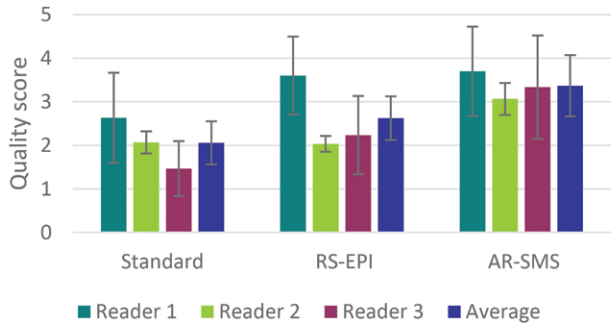

B

Method Comparison	Effect (95% CI)	p-value
RS-EPI vs. Standard	0.57 (0.36, 0.77)	<0.001*
AR-SMS vs. Standard	1.31 (1.10, 1.52)	<0.001*
AR-SMS vs. RS-EPI	0.74 (0.54, 0.95)	<0.001*

C

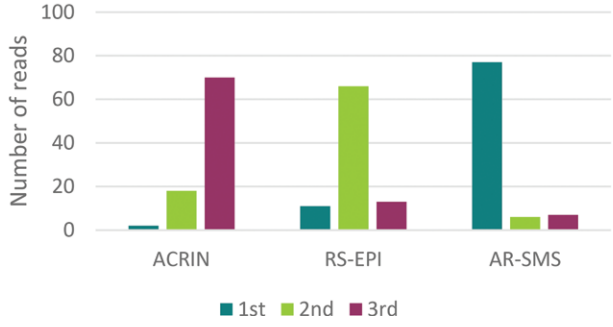

D

Method Comparison	Effect (95% CI)	p-value
RS-EPI vs. Standard	-0.73 (-0.89, -0.58)	<0.001*
AR-SMS vs. Standard	-1.53 (-1.69, -1.40)	<0.001*
AR-SMS vs. RS-EPI	-0.80 (-0.95, -0.65)	<0.001*

Figure 5: Summary of reader study results. *A*, Mean overall quality scores on a per-reader basis and, *B*, method comparison according to linear mixed-effects model accounting for participant and reader. Error bars, *A*, indicate standard error. Readers consistently scored axially reformatted (AR)–simultaneous multislice (SMS) imaging higher than readout-segmented (RS) echo-planar imaging (EPI) and standard spin-echo (SE) echo-planar imaging. *C*, Histogram of relative rank across all three readers and all lesions and, *D*, comparison of ranks according to linear mixed-effects model including *P* values. AR-SMS imaging was most frequently rated first, followed by RS echo-planar imaging at second. * Indicates statistical significance on the basis of Tukey-adjusted *P* values. ACRIN = American College of Radiology Imaging Network, CI = confidence interval.

A

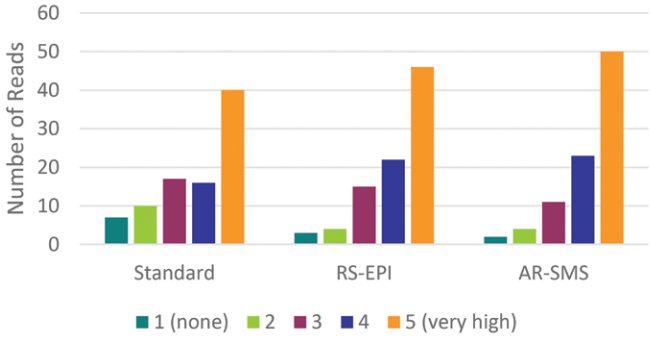

B

Method Comparison	Effect (95% CI)	p-value
RS-EPI vs. Standard	0.36 (0.15, 0.56)	0.002*
AR-SMS vs. Standard	0.48 (0.28, 0.68)	<0.001*
AR-SMS vs. RS-EPI	0.12 (-0.08, 0.32)	0.460

C

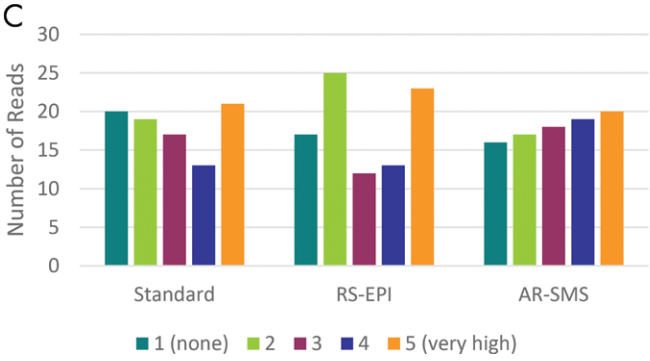

D

Method Comparison	Effect (95% CI)	p-value
RS-EPI vs. Standard	0.04 (-0.16, 0.25)	0.908
AR-SMS vs. Standard	0.16 (-0.05, 0.36)	0.309
AR-SMS vs. RS-EPI	0.11 (-0.10, 0.32)	0.296

Figure 6: Confidence of lesion size and apparent diffusion coefficient (ADC) measurements. Histograms of confidence ratings in measurement of, *A*, lesion size and, *C*, ADC on diffusion-weighted images (DWIs) across all readers and lesions. *B*, *D*, Method comparison represents the linear mixed-effects model accounting for participant and reader. Axially reformatted (AR)–simultaneous multislice (SMS) imaging was rated with the highest confidence in lesion size measurements on images with *b* values of 800 sec/mm^2, followed by, *B*, readout-segmented (RS) echo-planar imaging (EPI), and then standard spin-echo echo-planar imaging, with statistical significance. *D*, The ADC confidence did not depend on the DWI method. * Statistical significance indicated on the basis of Tukey-adjusted *P* values.

The intraclass correlation for overall image quality was poor to fair, indicating that each reader calibrated a unique internal scale. However, the linear mixed-effects model accounted for the reader and participant effects. The model found that AR-SMS outperformed RS echo-planar imaging, followed by standard SE echo-planar imaging in both image quality and rank (Fig 5). On the five-point Likert scale for image quality, RS echo-planar imaging rated an average of 0.57 points higher than standard SE echo-planar imaging ($P < .001$), and AR-SMS imaging scored 1.31 points higher than standard SE echo-planar imaging and 0.74 points higher than RS echo-planar imaging ($P < .001$). Similarly, on a scale of first to third place, AR-SMS ranked highest, followed by RS echo-planar imaging and standard SE echo-planar imaging as shown in Figure 5.

Histograms in Figure 6 indicate the number of reads rated with each confidence level for lesion size and ADC measurements, which reflects lesion measurability. There was higher confidence in the measurement of lesion size by using AR-SMS and RS echo-planar imaging compared with standard SE echo-planar imaging ($P < .001$ and $P = .002$, respectively); the comparison between AR-SMS and RS echo-planar imaging was not statistically significant. The method had no effect on the confidence in the measurement of lesion-average ADC ($P \geq .30$). See Figure 6 for details.

The statistical model indicated that lesion size played a role in the overall image quality scores ($P = .01$) independent of method ($P = .18$), indicating that the lesion size did not help to predict what method would be superior. Multiplicity was nine for 26 participants (one lesion, three readers, three methods) and 18 for two participants (two lesions, three readers, three methods).

Discussion

With growing interest in diffusion-weighted imaging (DWI) for breast cancer, it is vital to improve the image quality and spatial resolution of DWI methods. We compared three 5-minute protocols, standard spin-echo (SE) echo-planar imaging, readout-segmented (RS) echo-planar imaging, and axially reformatted (AR) simultaneous multislice (SMS) imaging. In both phantom and in vivo measurements, AR-SMS imaging outperformed RS echo-planar imaging and standard SE echo-planar imaging. Whereas both advanced methods have promise for improving clinical imaging, AR-SMS achieved larger anatomic coverage and better image quality than RS echo-planar imaging (0.74 points higher; $P < .001$).

Both RS echo-planar imaging and AR-SMS imaging have unique advantages and challenges. Practically, RS echo-planar imaging is more commonly available on clinical systems, and although general SMS methods are becoming more widespread, AR-SMS imaging is not commercially available currently. By increasing the number of segments, RS echo-planar images have reduced geometric distortion at the cost of imaging time. However, the RS echo-planar imaging protocol was limited in the anterior-posterior coverage, which prevented the inclusion of most lymph nodes. However, AR-SMS encoded a large imaging

volume quickly, which allowed for full coverage and a large number of averages and directions but required robust distortion correction. Combining the encoding speed of AR-SMS with the reduced distortion of RS echo-planar imaging may be a promising strategy for future work (21).

Our study had limitations. We used a subjective rating of image quality with expert readers because to our knowledge there is no objective reference standard for defining image quality. Although each reader interpreted the five-point Likert scale differently, the differences between the imaging methods were consistent. Further, we did not control all protocol parameters (ie, resolution, averages, volume coverage, and diffusion scheme) but rather optimized each method independently within a time constraint, as is performed clinically. All three methods could potentially be improved with further optimization, which limits the ability to generalize the study results.

The picture archiving and communication system software we used did not support colocalization of regions of interest across ADC maps and diffusion-weighted source images. Although readers rated the high-spatial-resolution methods with higher image quality and confidence in size measurements, the confidence in measuring ADCs did not change. With colocalization, we would expect the confidence in ADC measurement to increase similarly to that of lesion size measurement, which significantly improved for RS echo-planar imaging and AR-SMS imaging. The confidence in both lesion size and lesion-average ADC is likely to increase with additional experience with DWI in a clinical setting, especially for methods with higher spatial resolution.

In conclusion, the proposed axially reformatted simultaneous multislice imaging protocol provided higher spatial resolution and image quality than both the standard spin-echo echo-planar imaging breast diffusion-weighted imaging and a high-spatial-resolution readout-segmented echo-planar imaging approach, on the basis of phantom measurements and a reader study of in vivo imaging. Future work is needed to further compare specific protocols and compare the clinical performance of these techniques.

Author contributions: Guarantors of integrity of entire study, J.A.M., S.M., P.J.B.; study concepts/study design or data acquisition or data analysis/interpretation, all authors; manuscript drafting or manuscript revision for important intellectual content, all authors; approval of final version of submitted manuscript, all authors; agrees to ensure any questions related to the work are appropriately resolved, all authors; literature research, J.A.M., T.H.E., M.T.N., S.M., P.J.B.; clinical studies, J.A.M., M.T.N.; experimental studies, J.A.M., N.F.H., S.R., E.J.A., S.M., P.J.B.; statistical analysis, J.A.M., N.R., P.J.B.; and manuscript editing, all authors

Disclosures of Conflicts of Interest: **J.A.M.** disclosed no relevant relationships. **A.L.C.** disclosed no relevant relationships. **N.R.** disclosed no relevant relationships. **N.F.H.** disclosed no relevant relationships. **J.E.K.H.** disclosed no relevant relationships. **M.T.N.** disclosed no relevant relationships. **S.R.** Activities related to the present article: disclosed no relevant relationships. Activities not related to the present article: disclosed money paid to author for consultancy from the Medical University of South Carolina. Other relationships: disclosed no relevant relationships. **E.J.A.** Activities related to the present article: disclosed no relevant relationships. Activities not related to the present article: disclosed money paid to author for consultancy from Siemens Healthineers. Other relationships: disclosed no relevant relationships. **S.M.** disclosed no relevant relationships. **P.J.B.** disclosed no relevant relationships.

References

1. Iima M, Honda M, Sigmund EE, Ohno Kishimoto A, Kataoka M, Togashi K. Diffusion MRI of the breast: Current status and future directions. J Magn Reson Imaging 2019;52(1):70–90. https://doi.org/10.1002/jmri.26908.
2. Hirano M, Satake H, Ishigaki S, Ikeda M, Kawai H, Naganawa S. Diffusion-weighted imaging of breast masses: comparison of diagnostic performance using various apparent diffusion coefficient parameters. AJR Am J Roentgenol 2012;198(3):717–722.
3. Kang BJ, Lipson JA, Planey KR, et al. Rim sign in breast lesions on diffusion-weighted magnetic resonance imaging: diagnostic accuracy and clinical usefulness. J Magn Reson Imaging 2015;41(3):616–623.
4. Bogner W, Pinker-Domenig K, Bickel H, et al. Readout-segmented echo-planar imaging improves the diagnostic performance of diffusion-weighted MR breast examinations at 3.0 T. Radiology 2012;263(1):64–76. https://doi.org/10.1148/radiol.12111494.
5. Wisner DJ, Rogers N, Deshpande VS, et al. High-resolution diffusion-weighted imaging for the separation of benign from malignant BI-RADS 4/5 lesions found on breast MRI at 3T. J Magn Reson Imaging 2014;40(3):674–681.
6. Kim YJ, Kim SH, Kang BJ, et al. Readout-segmented echo-planar imaging in diffusion-weighted MR imaging in breast cancer: comparison with single-shot echo-planar imaging in image quality. Korean J Radiol 2014;15(4):403–410.
7. Kanao S, Kataoka M, Iima M, et al. High-resolution diffusion-weighted MRI of the breast using readout-segmented EPI and single-shot EPI. Imaging Med 2017;9(6):185–190. https://www.openaccessjournals.com/articles/highresolution-diffusionweighted-mri-of-the-breast-using-readoutsegmented-epi-and-singleshot-epi-12290.html.
8. Wilmes LJ, McLaughlin RL, Newitt DC, et al. High-resolution diffusion-weighted imaging for monitoring breast cancer treatment response. Acad Radiol 2013;20(5):581–589.
9. Singer L, Wilmes LJ, Saritas EU, et al. High-resolution diffusion-weighted magnetic resonance imaging in patients with locally advanced breast cancer. Acad Radiol 2012;19(5):526–534.
10. Taviani V, Alley MT, Banerjee S, et al. High-resolution diffusion-weighted imaging of the breast with multiband 2D radiofrequency pulses and a generalized parallel imaging reconstruction. Magn Reson Med 2017;77(1):209–220.
11. Setsompop K, Gagoski BA, Polimeni JR, Witzel T, Wedeen VJ, Wald LL. Blipped-controlled aliasing in parallel imaging for simultaneous multislice echo planar imaging with reduced g-factor penalty. Magn Reson Med 2012;67(5):1210–1224.
12. Moeller S, Yacoub E, Olman CA, et al. Multiband multislice GE-EPI at 7 tesla, with 16-fold acceleration using partial parallel imaging with application to high spatial and temporal whole-brain fMRI. Magn Reson Med 2010;63(5):1144–1153.
13. Larkman DJ, Hajnal JV, Herlihy AH, Coutts GA, Young IR, Ehnholm G. Use of multicoil arrays for separation of signal from multiple slices simultaneously excited. J Magn Reson Imaging 2001;13(2):313–317.
14. McKay JA, Moeller S, Ramanna S, et al. Nyquist Ghost Correction of High-Resolution SMS Breast DWI with Ghost/Object Minimization [abstr]. In: Proceedings of the Twenty-Seventh Meeting of the International Society for Magnetic Resonance in Medicine. Berkeley, Calif: International Society for Magnetic Resonance in Medicine, 2019; 3354.
15. Bolan PJ, Moeller S, Metzger GJ, et al. Breast Diffusion Weighted Imaging with Reduced Artifacts using Multi-band Spin Echo EPI [abstr]. In: Proceedings of the Twenty-Third Meeting of the International Society for Magnetic Resonance in Medicine. Berkeley, Calif: International Society for Magnetic Resonance in Medicine, 2015; 0884.
16. McKay JA, Moeller S, Ramanna S, et al. Comparison of methods for high spatial-resolution breast diffusion imaging [abstr]. In: Proceedings of the Twenty-Fifth Meeting of the International Society for Magnetic Resonance in Medicine. Berkeley, Calif: International Society for Magnetic Resonance in Medicine, 2017; 2115.
17. Keenan KE, Wilmes LJ, Aliu SO, et al. Design of a breast phantom for quantitative MRI. J Magn Reson Imaging 2016;44(3):610–619.
18. Partridge SC, Zhang Z, Newitt DC, et al. Diffusion-weighted MRI Findings Predict Pathologic Response in Neoadjuvant Treatment of Breast Cancer: The ACRIN 6698 Multicenter Trial. Radiology 2018;289(3):618–627.
19. Van Essen DC, Smith SM, Barch DM, et al. The WU-Minn Human Connectome Project: an overview. Neuroimage 2013;80:62–79.
20. Andersson JLR, Skare S, Ashburner J. How to correct susceptibility distortions in spin-echo echo-planar images: application to diffusion tensor imaging. Neuroimage 2003;20(2):870–888.
21. Filli L, Ghafoor S, Kenkel D, et al. Simultaneous multi-slice readout-segmented echo planar imaging for accelerated diffusion-weighted imaging of the breast. Eur J Radiol 2016;85(1):274–278.